Available online at www.sciencedirect.com

SciVerse ScienceDirect

Ceramics International 39 (2013) 4913–4921

CERAMICS INTERNATIONAL

www.elsevier.com/locate/ceramint

Comparative study on the sonophotocatalytic degradation of hazardous waste

Nasrin Talebian[a,*], Mohammad Reza Nilforoushan[b], Fatemeh Jazaeri Mogaddas[a]

[a]*Science Faculty, Department of Chemistry, Shahreza Branch, Islamic Azad University, Razi Chemistry Research Centre, Women Research Council, 86145-311, Shahreza, Isfahan, Iran*

[b]*Engineering Department, Sharekord University, Sharekord P.B. 115, Iran*

Received 3 November 2012; received in revised form 18 November 2012; accepted 26 November 2012
Available online 5 December 2012

Abstract

The enhanced sonophotocatalytic degradation of Chrome Intra Orange G (C.I. 18745), an azo dye, in aqueous solution under UV light has been carried out using solvothermally sensitized ZnO nanoparticles as catalyst. The effects of sonolysis, sonocatalysis, photocatalysis and sonophotocatalysis have been examined to study the influences on the degradation rates by varying the initial dye concentration, dye solution pH, catalyst morphology and loading to ascertain the synergistic effect on the degradation techniques. ZnO sonophotocatalysis was always faster than the respective individual processes. Ultrasound may modify the rate of photocatalytic degradation by promoting the deaggregation of the catalyst and ultrasound-induced increase of its active surface area, by increasing the amount of reactive radical species through cavitation leading to water splitting and formation of H_2O_2 by both photocatalysis and sonolysis. To further verify the direct relation of the effective surface area offered by ZnO to its reaction rate, sonophotocatalysis experiments were conducted using nanorods of different dimensions and aspect ratios. Higher aspect ratio values correspond to an enhancement of the sonophotocatalytic activity.

Keywords: Sonophotocatalysis; Azo dye degradation; Ultrasound; UV light

1. Introduction

Dye residuals found in textile dyeing wastewater contribute to the difficulty in treating such wastewater due to the increasing consumed amounts, variety and stability and resistance of modern dyes to biological destruction [1–3]. The efficient removal of dye pollutants from industrial wastewater can generally be achieved through heterogeneous photocatalysis using metal oxide semiconductors. Nevertheless, there are some drawbacks: (1) induction of non-modified catalyst only by ultraviolet light and costs lots of energy, (2) insufficient treatments of non- or low-transparent organic wastewaters and (3) ineffectiveness of conventional photocatalytic degradation methods for decolorization and mineralization. Due to these reasons, combinations of different advanced oxidation processes (AOP) for environmental detoxification have recently been exploited, especially for wastewater treatment [4]. The combination of ultrasound (US) and O_3 [5], UV [6], TiO_2 [7], H_2O_2 [8,9] or Fenton reagent [10,11] treatments, for example, is known to be able to increase the decomposition efficiency, to reduce the time required for pollutant removal and to verify possible beneficial or synergistic effects in the degradation of organic water pollutants.

Ultrasound irradiation results in acoustic cavitation, and bubble collapse causes intense local heating, high pressure and short lifetimes; these transient, localized hot spots lead to high energy chemical reactions [12]. This unique energy focusing process generates highly reactive free radicals that significantly enhance chemical processing. For instance, when water is irradiated with ultrasound, it is proved that the heat from cavity implosion decomposes water (H_2O) into extremely reactive hydrogen ions (H^+) and hydroxyl radicals ($OH^{\bullet -}$) [13,14]. During the quick cooling phase, hydrogen atoms and hydroxyl radicals recombine to form hydrogen peroxide (H_2O_2) and molecular hydrogen (H_2).

*Corresponding author. Tel.: +98 321 329 2260; fax: +98 321 3232701.
E-mail addresses: nasrin_talebian@yahoo.com, talebian@iaush.ac.ir (N. Talebian).

0272-8842/$ - see front matter © 2012 Elsevier Ltd and Techna Group S.r.l. All rights reserved.
http://dx.doi.org/10.1016/j.ceramint.2012.11.085

If other compounds are added to water irradiated with ultrasound, a wide range of secondary reactions can occur. Organic compounds are highly degraded in this environment, and inorganic compounds can be oxidized or reduced [15].

Anbar and Pecht [16] investigated the location of the sonochemical formation of hydrogen peroxide and found that H_2O_2 is produced in the cavitation bubbles and not in the liquid phase. Suslick et al. investigated the application of sonochemistry in numerous commercial processes and found that either better quality of the products were achieved or simpler experimental conditions were required when ultrasound was introduced [17–19].

The potential applications of this technology range from degradation of environmental pollutants to drug synthesis for medical treatments. Especially, it is suitable to treat those organic wastewaters that cannot be degradated by photocatalytic technology. In recent years, the simultaneous use of ultrasound and photocatalysis, i.e. the so-called sonophotocatalysis has been studied regarding process efficiency to degrade various organics in model solutions [20–24]. The sonophotocatalytic process of oxidation shows interesting advantages at kinetic level, due to the occurance of a synergistic effect between sonolysis and photocatalysis [20–24]. Synergistic effects between the two techniques were observed when employing small particle size semiconductors [23] or when operating at relatively low US frequency (30 kHz) [25,26].

Reports on heterogeneous sonophotocatalysis under different experimental conditions are available in literature [27–33]. There are also many reports on morphology-dependent of photocatalytic activity of certain catalyst especially ZnO nanostructures [34–37]. However, to our knowledge, no work has been reported on the comparative study of the effect of ZnO nanoparticles morphology particularly resulted from solvothermally synthesis on the sonophotocatalytic reactivity.

In this paper, sonolysis and photocatalysis have been simultaneously employed to degrade selective an azo dye, Chrome Intra Orange G (C.I. 18745). We report the synthesis of nanostructure ZnO rod-like with different aspect ratio by simple solvothermal methods. ZnO materials with different crystal growth habits showed significant differences in catalytic performance. The aim of this work is to study the influence of the substrate concentration, photocatalyst morphology and its optimum loading, and pH on the azo dye degradation rate to exploit the synergistic effect between different combined applications. The results indicated that the surface morphology, size and surface area of ZnO nanorod arrays were key factors influencing the efficiency of ZnO in the degradation of azo dye.

2. Experimental

2.1. Materials and methods

The commercially available dye Chrome Intra Orange G was obtained as a gift sample from an Iran textile industry, and used as such without any purification. Required concentrations of dye solutions were prepared by dissolving the dye in distilled water. The pH of the solutions was adjusted by adding 1 M HNO_3 or 1 M NaOH. The molecular structure of dye is shown in Scheme 1. The ultrasonic bath operated at frequency of 30 kHz and output power of 50 W through manual adjustment. All systems were at continuous stirring; additionally, the temperature was controlled at 30 °C via a water circulation system. In a typical heterogeneous catalytic run, the appropriate amount of ZnO was added in the reaction mixture and the suspension was left for 15 min in the dark to ensure complete equilibration of adsorption/desorption of the dye compound on the catalyst surface. After that period of time, the lamp and/or the sonicator were turned on and this was taken as "time zero" for the reaction. Illumination was performed through the reactor Pyrex walls by means of four 8 W Phillips UV-A lamps emitting 365 nm wavelength. Aliquots were withdrawn from the reactor at pre-specified time intervals. The suspended particles were separated by filtering. The degradation reaction was monitored by spectrophotometric analysis at the absorption maximum of the dye.

2.2. Synthesis of ZnO powders

In a typical synthesis [38], 0.01 mol of $Zn(Ac)_2 \cdot 2H_2O$ powders were placed into a Teflon-lined stainless steel autoclave of 50 ml capacity, to which 40 ml of 5 wt%, 40 wt% and 80 wt% hydrazine hydrate aqueous solutions were added with stirring. The autoclave was maintained at 90 °C for 12 h, then air cooled to room temperature. The as-formed white precipitate was filtered, washed with distilled water, and dried in the air at 80 °C.

2.3. Apparatus

To characterize the ZnO powders, X-ray power diffraction (XRD) experiments were performed on a Bruker, D8 ADVANCEXRD diffraction spectrometer with a Cu Kα line at 1.5406 Å and a Ni filter for an angle range of $2\theta = 20–80°$. Philips, XL30 scanning electron microscope (SEM) measurements were also used to investigate the morphology of the samples with an accelerating voltage of 17 kV. The optical properties were performed on a Shimadzu, MPC-2200 UV–vis spectrophotometer operated over the range of 350–600 nm at a resolution of 2.0 nm.

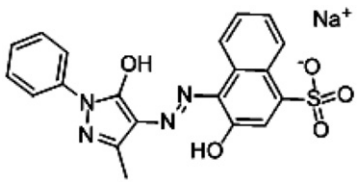

Scheme 1. Chemical structure of chrome intra orange G.

3. Results and discussion

3.1. Characterization

Fig. 1 shows the XRD patterns of the obtained products using hydrazine hydrate aqueous solutions as the solvent. All the obtained products display the characteristic XRD peaks corresponding to the hexagonal phase (space group: P63mc) of ZnO (Joint committee for Powder Diffraction Standards (JCPDS) file no. 36-1451). Furthermore, as observed from XRD pattern intensities, the higher content of hydrazine hydrate in the solvent can generally enhance the crystallinity of the obtained ZnO powders. For abbreviation, the ZnO samples prepared in 5 wt%, 40 wt% and 80 wt% hydrazine hydrate aqueous solutions labeled by sample 1, sample 2 and sample 3, respectively. The grain size was calculated from wurzite (002) reflection, using the Scherrer equation. The average grain size is 55, 73 and 96 nm for sample 1, 2 and 3, respectively.

SEM images of the as-prepared ZnO powders are shown in Fig. 2. The prepared ZnO samples using the hydrazine hydrate aqueous solutions with 5 wt%, 40 wt% and 80 wt% consist of granular, hexagonal granular as well as hexagonal rod-like

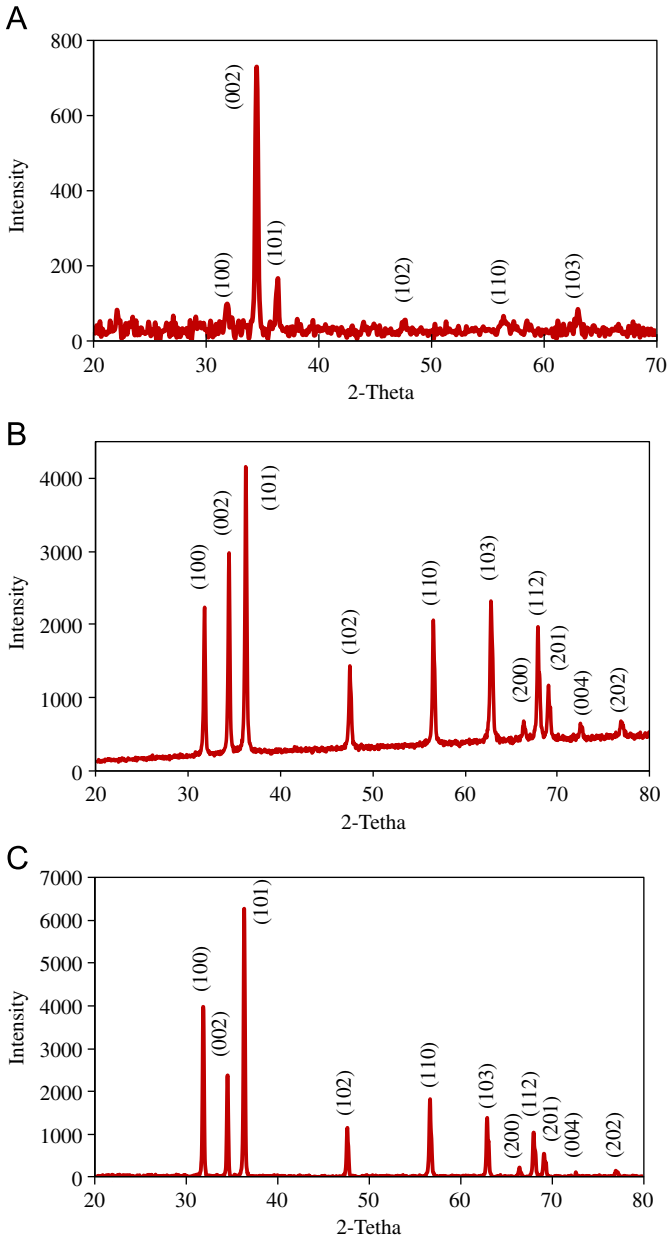

Fig. 1. XRD patterns of the as-prepared ZnO products using the hydrazine hydrate aqueous solutions with different concentrations: (A) 5 wt%, (B) 40 wt% and (C) 80 wt%.

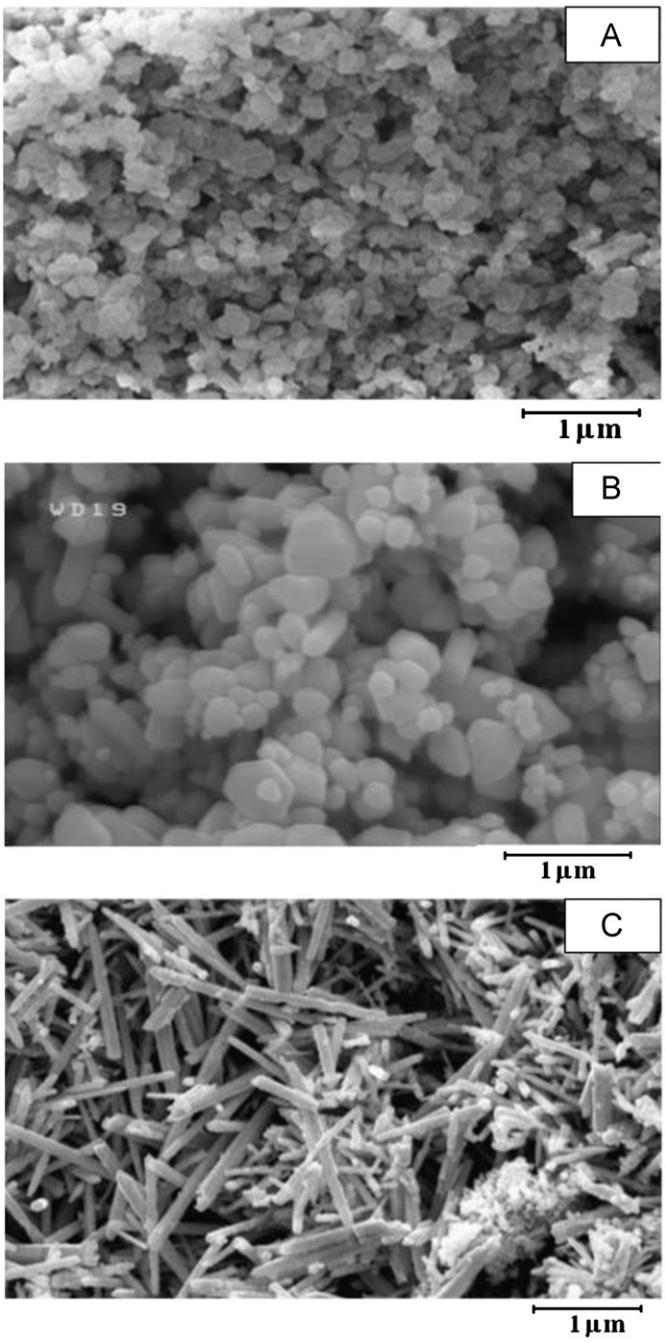

Fig. 2. SEM images of the obtained ZnO powders using the hydrazine hydrate aqueous solutions with different concentrations: (A) 5 wt%, (B) 40 wt% and (C) 80 wt%.

particles and pure individual ZnO nanorods, respectively. During the solvothermal process, hydrazine hydrate played important roles as a basic and complexing reagent in the nucleation and growth of the ZnO products. It not only can provide hydroxyl anions by hydrolyzation, but it can also coordinate with Zn^{2+} cations to form a weak coordination compound, $[Zn(N_2H_4)_2]^{2+}$ [39]. It was suggested that the existing competitive reactions forming different species such as $Zn(OH)_4^{2-}$, $Zn(OH)_2$ and $[Zn(N_2H_4)_2]^{2+}$ lead to the variation of the ZnO morphologies with the contents of the solvents [40–42].

The initially formed $Zn(OH)_2$ in low concentration (5 wt%) hydrazine hydrate aqueous solution, can quickly dehydrate to give large quantities of ZnO nuclei upon hydrothermal treatment at 90 °C, which led to the mainly granular particles [40]. On the other hand, in high concentration (80 wt%) hydrazine hydrate aqueous solutions, ZnO crystal gradually formed, the number of nuclei was limited and the particle size increased through progressive growth. For the hydrothermal crystal growth process of ZnO in a high alkali aqueous solution, the growth unit is $[Zn(OH)_4^{2-}]$ [40,41]. With increasing concentration of $[Zn(OH)_4^{2-}]$ in the solution, these ions prefer to aggregate at more positive polar planes of ZnO crystals due to the electrostatic forces, which would retard the growth along the [0001] direction greatly and result in the formation of nanorods with a higher aspect ratio [42,43]. Moreover, the hydrazine hydrate may serve as chelating (adsorbing) ligands to the Zn^{2+} cations (primarily on the six prismatic side planes), inhibiting the radial enlargement of the rods [44]. Considering the above factors, individual ZnO nanorods were obtained in the high concentration (80 wt%) of hydrazine hydrate aqueous solutions as previously reported [38]. However, at intermediate concentration (40 wt%) of hydrazine hydrate aqueous solutions, nucleation and growth processes could occur at the same time and then, both granular and rod-like particles generate upon hydrothermal treatment.

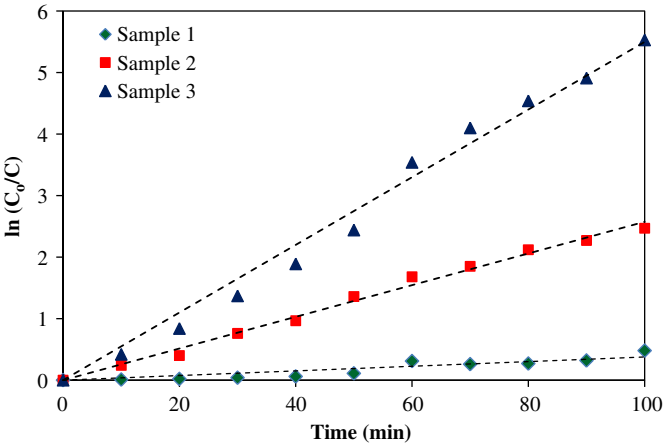

Fig. 3. Effect of catalyst on the azo dye degradation during sonocatalysis with 0.5 g L^{-1} ZnO and C_0=10 mg L^{-1}.

3.2. Sonolytic (US) and sonocatalytic (US+ZnO) degradation of azo dye

Fig. 3 shows the effect of catalyst on the sonocatalytic degradation kinetics of azo dye as a function of the sonication time, at 10 mg L^{-1} initial dye concentration. The rate constants increase during sonocatalysis compared to sonolysis showing clearly the beneficial effect of the presence of catalyst on azo dye degradation (see Table 1). It is expected that suspended solids affect cavitation and consequently the rate of sonochemical degradation. In principle, particles may enhance degradation providing additional nuclei for bubble formation [45].

3.3. Photocatalytic (UV+ZnO) and sonophotocatalytic (US+UV+ZnO) degradation of azo dye

Like sonolysis, photocatalysis and sonophotocatalysis also appear to follow a pseudo-first order kinetics. Table 1 shows values of initial rate constants during the degradation of azo dye at an initial concentration of 10 mg L^{-1} for different treatments. As clearly seen, photocatalytic degradation occurs appreciably faster than sonolytic or sonocatalytic degradation under similar experimental conditions. For instance, complete photocatalytic dye removal occurs within 40 min of reaction at 0.5 g L^{-1} catalyst loading under air, while sonolysis or sonocatalysis achieve up to 45 and 88% efficiencies at 100 min of reaction, respectively. Synergistic effects have been evidenced by comparing kinetic results obtained by sonolytic, sonocatlytic, photocatalytic and sonophotocatalytic treatments. The synergy between different treatments can be usefully quantified by the following equation and values given in Table 1:

$$\text{Synergy} = \frac{k(\text{US}+\text{UV}+\text{ZnO})}{k(\text{US})+k(\text{US}+\text{ZnO})+k(\text{UV}+\text{ZnO})}$$

Table 1
Azo dye degradation rate constants at 10 mg L^{-1} starting concentration and various treatment conditions.

Rate constant (min^{-1})	Condition	Rate constants (min^{-1})			
US	Catalyst	US+ZnO	UV-A+ZnO	US+UV+ZnO	Synergy
0.811	Sample 1	33.8	14.5	54.2	2.82
7.31	Sample 2	25.8	79.2	125	1.11
15.6	Sample 3	55.1	192	562	2.14

where k(US+UV+ZnO), k(US), k(UV+ZnO) and k(US+ZnO) are initial rate constants for sonophotocatalytic, sonolytic, photocatalytic, and sonocatalytic degradation, respectively.

As indicated from the calculated synergy values larger than 1.0, a synergistic effect was seen. The combined effect of sonolysis and photocatalysis led to a degradation rate constant ($k_{US+UV+ZnO}$) which was greater than the sum of the degradation rate constants measured under sonolysis (k_{US}), photocatalysis (k_{UV+ZnO}) and sonolysis (k_{US+ZnO}).

The main mechanism for the enhanced sonophotocatalytic destruction of azo dye was most likely due to: (1) additional free radicals formed from the decomposition or pyrolysis of H_2O in a cavitation bubble, (2) additional produced hydrogen peroxide by both photocatalysis and sonolysis in water: under photocatalysis via reduction of adsorbed dioxygen by conduction band electrons [46] and under sonolysis of water as a result of recombination between hydroxyl radicals produced by the implosion of cavitation bubbles [47,48], (3) hydroxyl radical-mediated reactions occurring primarily in the liquid bulk as well as at the bubble interface due to non-volatility and highly solubility of the azo dye, (4) deaggregation of particles due to the effect of sonication leading to an increase in surface area, (5) the use of ultrasound creates conditions of increased turbulence in the liquid, thus decreasing mass transfer limitations and increasing the surface area available due to catalyst fragmentation and de-agglomeration [49] and finally (6) synergic effects of photocatalysis and sonolysis on the degradation.

3.4. Influence of morphology of ZnO powders on sonophotocatalytic activity

The properties of ZnO are strongly dependent on its structure, including the morphology, aspect ratio, size, orientation, and density of crystal [50–52]. Taking into consideration the nanorods' dimensions obtained from SEM, i.e., their diameter and length, we can estimate the aspect ratio (length over diameter, L/D) of the ZnO samples. (L/D) is a commonly used parameter which indicates the surface-to-volume ratio of nanostructured samples. The high aspect ratio (~14.3–17.5) and enhanced crystallinity of the sample 3 compared to sample 2 (~4.3–6.5) and sample 1 (~1.2–2.4) result in significant sonophotocatalytic activity of former. In addition to higher dye adsorption due to increased surface-to-volume ratio of sample 3, a number of other physical processes can occur in the presence of particles during sonication. For example, particles may serve as nucleation sites for cavitation bubbles. Then, slight to moderate increases in the reaction rate constants during all degradation methods as the particle size, aspect ratio and morphology change were observed. The exposed surface area and the defects on the surface are also important parameters which affect the photocatalytic activities of metal oxide semiconductors. Due to higher aspect ratio, ZnO nanorods expose more surface defects to degrade organic pollutants.

3.5. Influence of initial concentration on sonophotocatalytic degradation of chrome Intra orange G

It is important to study the dependence of degradation efficiency on the initial concentration of dye wastewater from both application and comparative point of view. The reaction kinetics was studied by varying initial concentration of dye in suspensions containing 0.5 g L^{-1} of ZnO at pH of 4. The degradation rate of dye measured under different experimental conditions is shown in Fig. 4. The decrease in reaction rate with increase in substrate concentration is due to (1) increasing of dye molecules adsorbed on the surface of catalyst hampers the absorption of UV-light and high energies resulted from ultrasonic cavitation effect by catalyst, (2) limited the catalytic activity of any catalyst and saturation of its degradation ability, (3) suppress the synergistic effect at higher concentrations and (4) the constancy of the amount of substrate adsorbed on the semiconductor at higher concentrations. As observed from Fig. 4, there are the same trends for all degradation treatments, i.e., the simultaneous sonolysis did not induce any modification in this trend, indicating that the reaction system exhibits the same dependence on the amount of dye under both photocatalytic and sonophotocatalytic conditions, which determines the water-semiconductor interface phenomena [53].

3.6. Influence of solution acidity on sonophotocatalytic degradation of azo dye

Some organic compounds exhibit a wide variation in speciation (or charge) and physico-chemical properties at different pH conditions. Besides, the pH of an aquatic environment plays an important role on the photocatalytic degradation of organic contaminants since it determines the surface charge of the photocatalyst and the size of aggregates it forms [54,55]. Therefore, the pH of the solution can play a key role in the adsorption and photocatalytic oxidation of pollutants. The effect of pH value in range from 3.0 to 10.0 on the sonophotocatalytic

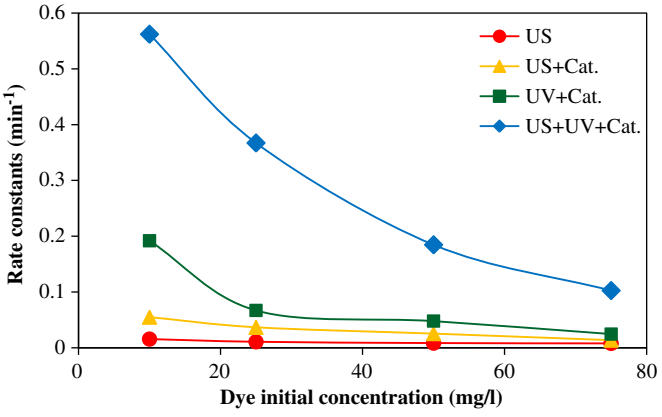

Fig. 4. Rate constants of the degradation of azo dye, as a function of the initial dye concentration under deferent treatments.

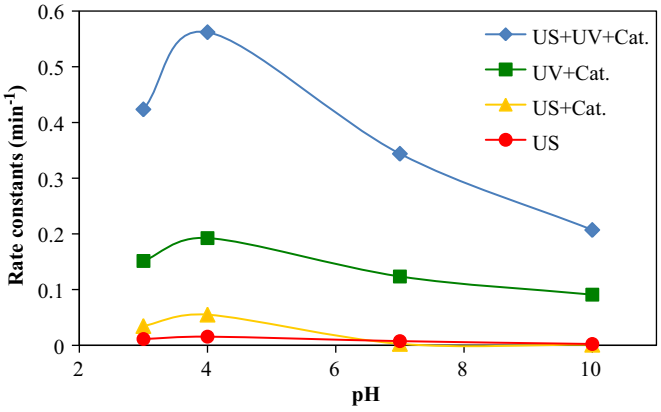

Fig. 5. Influence of pH on kinetics of various treatment conditions for azo dye degradation after 6 min UV illumination.

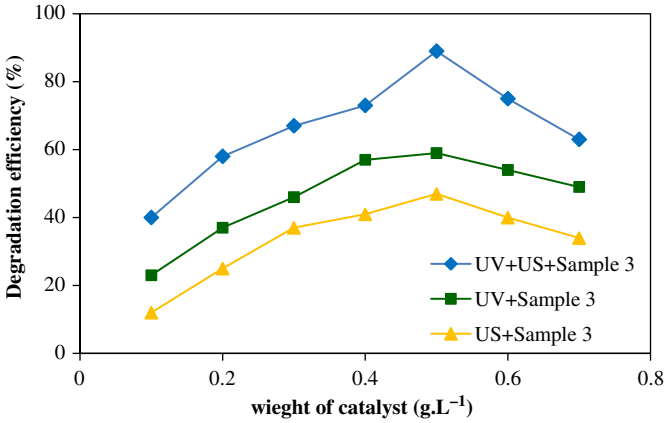

Fig. 6. Influence of ZnO loading (sample 3) on the sonophotocatalytic, photocatalytic and sonocatalytic degradation efficiency.

degradation was investigated and the kinetics results are shown in Fig. 5.

The degradation rates reached a maximum in acidic conditions, followed by a decrease in the pH range from 7 to 10. The same trend is seen in the various treatment conditions. From the higher degradation efficiency in acidic medium, any changes in the initial degradation rate with varying pH values must be ascribed to variations of the acid/base properties of the ZnO particles surface (pzc∼8.8) and its relation to the acid dissociation constants of dye. As a result of electrostatic attraction of the positively charged ZnO with the ionized dye, an increase in the reaction rate has been observed in acidic solution.

3.7. Influence of catalyst amount

Understanding the impacts of catalyst loading on the photocatalytic degradation efficiency is of paramount importance from commercially point of view. As the suspension of catalyst loading increases, this change may affect the photocatalytic degradation efficiency due to: (1) increasing the availability of active sites, (2) decreasing the light penetration, (3) deactivation of activated dye molecules by collision with molecules in ground state [56] and (4) agglomeration of the ZnO particles.

In (2)–(4) conditions, part of the catalyst surface has probably became unavailable for photon absorption as well as dye adsorption, thus photo-induced excitation slightly occurs resulting to the lower degradation efficiency. As shown in Fig. 6, higher sonophotocatalytic, photocatalytic and sonocatalytic efficiencies were observed with increasing sample 3 amounts, up to an optimal ZnO amount of 0.5 g L^{-1}, followed by a marked decrease at higher catalyst amounts.

3.8. Dye degradation intermediates and possible reaction mechanism

Since photocatalysis is a surface phenomenon, a critical intervening step in the effectiveness of a given pollutant photodegradation is to understand the adsorption process of pollutant on the catalyzing surface. Studying the adsorbability of the organic substrate allows one to predict the mechanism and kinetics that promote the pollutant's photo-oxidation. In present work, this was established by FTIR spectroscopy. Fig. 7 shows typical spectra of ZnO nanoparticles (sample 3, Fig. 7A) and the adsorbed azo dye before (Fig. 7B) and after 2, 4 and 6 min UV/US irradiation during sonophotocatalytic degradation, Fig. 7C, D and E, respectively.

The dye degradation occurred mainly by: (1) photocatalytic oxidation through the hydroxyl radical attack and the hydroxylation of the aromatic ring [57], (2) direct oxidation or reduction by the photo-induced holes and electrons, respectively, resulting to desulfonation and oxidative cleavage of the azo bond [58–61]. Then, the major identified intermediates are hydroxylated derivatives, aromatic amines, naphthoquinone, phenolic compounds, and some aldehydes as precursor of produced carboxylic acids [62].

Fig. 7(A) shows the intense Zn–O characteristic bands of bared ZnO around 780–830 cm^{-1}. The peaks around 3450 cm^{-1} represent surface hydroxyl groups. It is well established that a surface-bound hydroxyl group behaves as 'surface zincanol' (ZnO…$OH^{\bullet}$), which is ultimately responsible for the degradation [63].

The new bands appear in the characteristic region of azo dye compounds due to dye adsorption on the catalyst surface before UV irradiation in Fig. 8(B). The bands situated at 1194, 1106 and 1023 cm^{-1} were characteristic of the asymmetric stretching vibration in the $–SO_3Na$ group and of the coupling between the benzene mode and $\upsilon(SO_3)$ [63], while the peak located at 1345 cm^{-1} could be either ascribed to O–H bending vibrations or to SO_2–O fingerprint. The intense peaks near 1421 and 1536 cm^{-1} were attributed to the –N=N– bond [64] and to the aromatic ring vibrations sensitive to the interaction with the azo bond [58,65], or to the bending vibration mode δ(N–N) of the hydrazone form of the azo dye [66].

After this, sample 3 was UV/US irradiated for 2, 4 and 6 min. The presence of carbonyl groups (especially

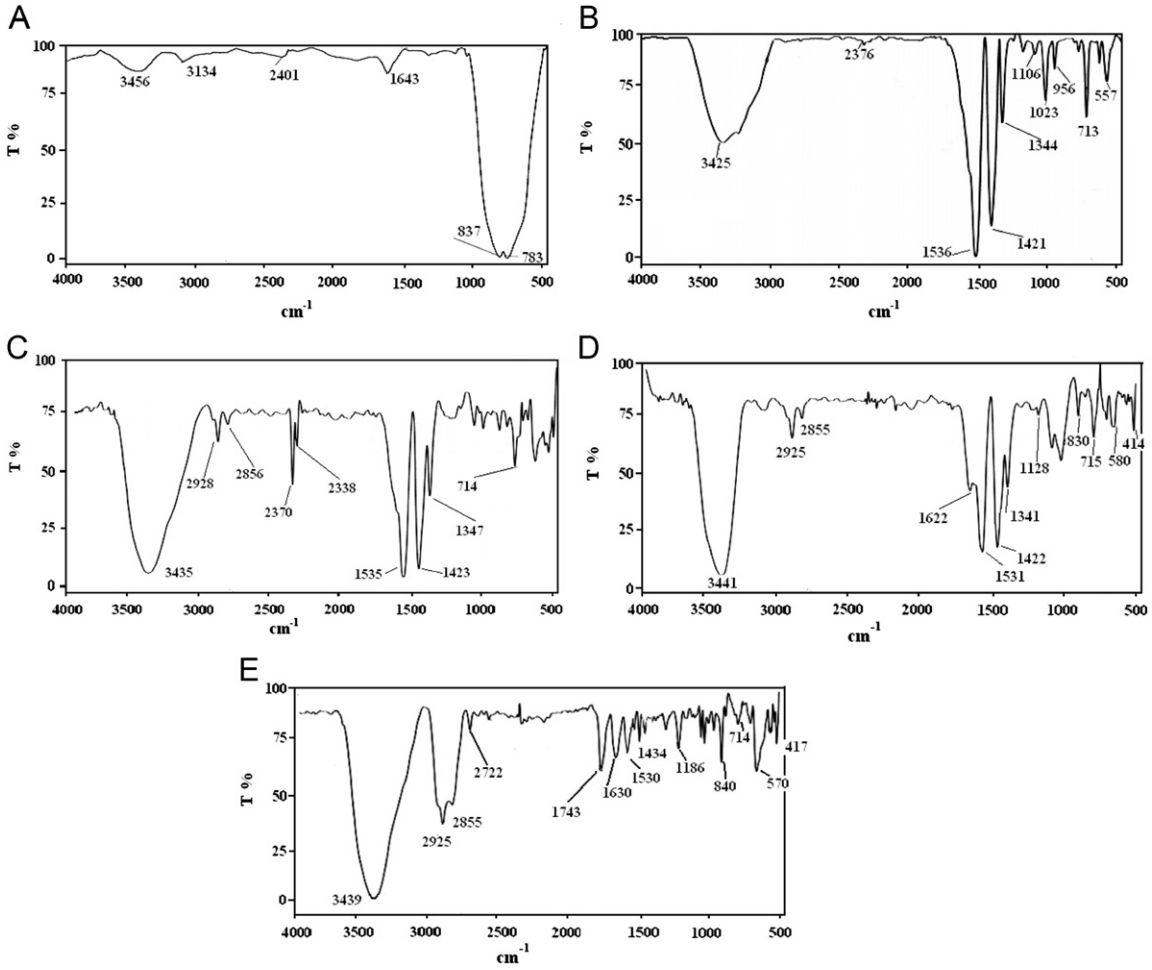

Fig. 7. FTIR of (A) ZnO nanorods (sample 3), (B) azo dye adsorbed on ZnO surface after 15 min in dark condition, and azo dye adsorbed on ZnO surface after (C) 2 min, (D) 4 min and (E) 6 min at sonophotocatalytic treatment.

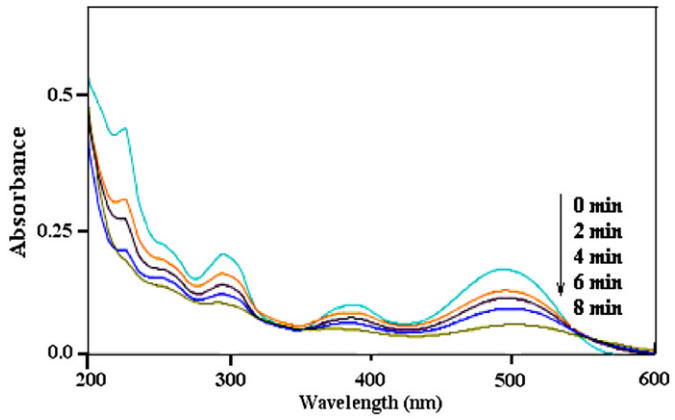

Fig. 8. UV–vis spectra of chrome intra orange G solution under sonophotocatalytic condition using sample 3 as catalyst at 0–8 min time intervals.

aldehyde, as a precursor of carboxylic acid) is indicated by the absorption maxima around 1620–1740 cm^{-1} and 2855–2926 cm^{-1}. At longer irradiation times (6 min), the intensity of these bands is increased and that of characteristic bands of the azo dye is strongly decreased. Two peaks around 1630 and 1743 cm^{-1} with a considerable fractional transmittance in Fig. 7(E) clearly suggest the formation of carboxylic acid groups as a result of attack by the oxidizing radicals.

Under photocatalytic conditions, a set of reactions in presence of water molecules and dissolved oxygen follow leading to the formation of several active oxygen species such as superoxide anion, hydroperoxyl radical besides hydroxyl radical. The main active species, $^{\bullet}OH$, free or adsorbed on the catalyst surface, designated as active 'zincanol ($ZnO\ldots OH^{\bullet}$)', may attack azo dye to produce a $DYE^{\bullet}$ radical that undergoes degradation to yield products. The increased intensity of band around 3440 cm^{-1} at longer irradiation times is assigned to OH binding and stretching of the adsorbed water on the catalyst surface. Results indicate that the photocatalytic degradation of the azo dye may occur by means of their direct reaction with holes or $^{\bullet}OH$ radicals to yield the corresponding aldehydes. The aldehydes generated in these reactions may respectively react with $O_2^{\bullet-}$ or $^{\bullet}OH$ radicals, to yield the corresponding carboxylates or carboxylic acids.

3.9. UV–vis spectra of chrome intra orange G solutions during sonophotocatalytic degradation

Fig. 8 shows the UV–vis spectra of chrome intra orange G solution under sonophotocatalytic treatment using sample 3 as catalyst at different illumination times and at optimized conditions including initial dye concentration $10\,mg\,L^{-1}$, $0.5\,g\,L^{-1}$ of ZnO powder loading and solution pH = 4. In general, the chrome intra orange G solution gives three main absorption peaks in the range of 200–600 nm, corresponding to the benzene ring and azo bond, respectively. It was found that, compared with the original dye solution ($t = 0$ min), all absorption peaks declined more or less due to the sonophotocatalytic degradation. It indicates that the benzene ring and azo bond in dye molecule are degraded simultaneously.

4. Conclusion

Effective destruction of the azo dye, chrome intra orange G is possible by combinative AOPs in the presence of ZnO suspensions, UV light and sonolysis. The kinetics of the sonolytic, sonocatalytic, photocatalytic and sonophotocatalytic oxidation follows a Langmuir–Hinshelwood model and depends on several factors such as, dye concentration, mass of catalyst, solution pH, and morphology of ZnO powders. Ultrasound improves the rate of the photocatalytic degradation of azo dye, through a synergistic effect between sonolysis and photocatalysis. This increases the amount of reactive radical species through cavitation and H_2O_2 production. Experimental results concerning the US/UV/ZnO system suggested that US also accelerated mass transfer between the solution phase and the ZnO surface, increasing the degradation kinetics. It is found that the different surface areas offered by ZnO samples with different dimensions and aspect ratios could be considered as key factor in the their sonophotocatalytic activities.

References

[1] R. Ullah, J. Dutta, Photocatalytic degradation of organic dyes with manganese-doped ZnO nanoparticles, Journal of Hazardous Materials 156 (2008) 194–200.

[2] I. Arslan-Alaton, B.H. Gursoy, J.E. Schmidt, Advanced oxidation of acid and reactive dyes: effect of fenton treatment on aerobic, anoxic and anaerobic processes, Dyes and Pigments 78 (2008) 117–130.

[3] M.T. Michael, M.G. Georg, R. Astrid, Degradation of azo dyes by oxidative processes—laccase and ultrasound treatment, Bioresource Technology 99 (2008) 4213–4220.

[4] R. Andreozzi, V. Caprio, A. Insola, R. Marotta, Advanced oxidation processes (AOP) for water purification and recovery, Catalysis Today 53 (1999) 51–59.

[5] G. Tezcanli-Guyer, N.H. Ince, Individual and combined effects of ultrasound, ozone and UV irradiation: a case study with textile dyes, Ultrasonics 42 (2004) 603–609.

[6] E. Naffrechoux, S. Chanoux, C. Petrier, J. Suptil, Sonochemical and photochemical oxidation of organic matter, Ultrasonics Sonochemistry 7 (2000) 255–259.

[7] J. Wang, T. Ma, Z. Zhang, X. Zhang, Y. Jiang, D. Dong, P. Zhang, Y. Li, Investigation on the sonocatalytic degradation of parathion in the presence of nanometer rutile titanium dioxide (TiO_2) catalyst, Journal of Hazardous Materials 137 (2006) 972–980.

[8] D.B. Voncina, A. Majcen-Le-Marechal, Reactive dye decolorization using combined ultrasound/H_2O_2, Dyes and Pigments 59 (2003) 173–179.

[9] M. Dukkanci, G. Gunduz, Ultrasonic degradation of oxalic acid in aqueous solutions, Ultrasonics Sonochemistry 13 (2006) 517–522.

[10] J.-T. Li, Y.-L. Song, Degradation of AR 97 aqueous solution by combination of ultrasound and Fenton reagent, Environmental Progress & Sustainable Energy 29 (2010) 101–106.

[11] Y.-S. Ma, C.-F. Sung, J.-G. Lin, Degradation of carbofuran in aqueous solution by ultrasound and Fenton processes: effect of system parameters and kinetic study, Journal of Hazardous Materials 178 (2010) 320–325.

[12] K.S. Suslick, in: Ultrasound: its chemical, physical and biological effects, VCH, New York, 1988.

[13] K.S. Suslick, The chemical effects of ultrasound, Scientific American 260 (2) (1989) 62–68.

[14] P. Riesz, T. Kondo, Free radical formation induced by ultrasound and its biological implications, Free Radical Biology and Medicine 13 (1992) 247–270.

[15] K. Makino, M.M. Mossoba, P. Riesz, Chemical effects of ultrasound on aqueous solutions. For ation of hydroxyl radicals and hydrogen atoms, Journal of Physical Chemistry 87 (1983) 1369–1377.

[16] M. Anbar, I. Pecht, On the sonochemical formation of hydrogen peroxide in water, Journal of Physical Chemistry 68 (1964) 352–355.

[17] T. Hyeon, M. Fang, K.S. Suslick, nanostructured molybdenum carbide: sonochemical synthesis and catalytic properties, Journal of the American Chemical Society 118 (1996) 5492–5493.

[18] K.S. Suslick, S.B. Choe, A.A. Cichowlas, M.W. Grinstaff, Sonochemical synthesis of amorphous iron, Nature 353 (1991) 414–416.

[19] K.S. Suslick, S.J. Doktycz, E.B. Flint, On the origin of sonoluminescence and sonochemistry, Ultrasonics 28 (1990) 280–290.

[20] S. Matzusawa, J. Tanaka, S. Sato, T. Ibusuki, Photocatalytic oxidation photocatalytic oxidation of dibenzothiophenes in acetonitrile using TiO_2: effect of hydrogen peroxide and ultrasound irradiation, Journal of Photochemistry and Photobiology A: Chemistry 149 (2002) 183–189.

[21] Y. Kado, M. Atobe, T. Nonaka, Ultrasonic effects on electroorganic processes—part 20 Photocatalytic oxidation of aliphatic alcohols in aqueous suspension of TiO_2 powder, Ultrasonics Sonochemistry 8 (2001) 69–74.

[22] E. Selli, Synergistic effects of sonolysis combined with photocatalysis in the degradation of an azo dye, Journal of Physical Chemistry Chemical Physics 4 (2002) 6123–6128.

[23] L. Davydov, E.P. Reddy, P. France, P.G. Smirniotis, Sonophotocatalytic destruction of organic contaminants in aqueous systems on TiO_2 powders, Applied Catalysis B: Environmental 32 (2001) 95–105.

[24] M. Mrowetz, E. Selli, C. Pirola, Degradation of organic water pollutants through sonophotocatalysis in the presence of TiO_2, Ultrasonics Sonochemistry 10 (2003) 247–254.

[25] C. Drosou, A. Coz, N.P. Xekoukoulotakis, A. Moya, Y. Vergara, D. Mantzavinos, Peracetic acidenhanced photocatalytic and sonophotocatalytic inactivation of *E. coli* in aqueous suspensions, Journal of Chemical Technology & Biotechnology 85 (8) (2010) 1049–1053.

[26] P. Theron, P. Pichat, C. Guillard, C. Petrier, T. Chopin, Degradation of phenyl trifluoro methyl ketone in water by separate or simultaneous use of TiO_2 photocatalysis and 30 or 515 kHz ultrasound, Journal of Physical Chemistry Chemical Physics 1 (1999) 4663–4668.

[27] Y. He, F. Grieser, M. Ashokkumar, The mechanism of sonophotocatalytic degradation of methyl orange and its products in aqueous solutions, Ultrasonics Sonochemistry 18 (5) (2011) 974–980.

[28] B. Neppolian, L. Ciceri, C.L. Bianchi, F. Grieser, M. Ashokkumar, Sonophotocatalytic degradation of 4-chlorophenol using $Bi_2O_3/TiZrO_4$ as a visible light responsive photocatalyst, Ultrasonics Sonochemistry 18 (1) (2011) 135–139.

[29] S. Wang, Q. Gong, J. Liang, Sonophotocatalytic degradation of methyl orange by carbon nanotube/TiO_2 in aqueous solutions, Ultrasonics Sonochemistry 16 (2) (2009) 205–208.

[30] H. Harada, C. Hosoki, A. Kudo, Overall water splitting by sonophotocatalytic reaction: the role of powdered photocatalyst and an attempt to decompose water using a visible light sensitive photocatalyst, Journal of Photochemistry and Photobiology A: Chemistry 141 (2001) 219–224.
[31] M. Mrowetz, C. Pirola, E. Selli, Degradation of organic water pollutants through sonophotocatalysis in the presence of TiO_2, Ultrasonics Sonochemistry 10 (2003) 247–254.
[32] I.Z. Shirgaonkar, A.B. Pandit, Sonophotochemical destruction of aqueous solution of 2,4,6-trichlorophenol, Ultrasonics Sonochemistry 5 (1998) 53–61.
[33] N.L. Stock, J. Peller, K. Vinodgopal, P.V. Kamat, Combinative sonolysis and photocatalysis for textile dye degradation, Environmental Science and Technology 34 (2000) 1747–1750.
[34] X.G. Han, H.Z. He, Q. Kuang, X. Zhou, X.H. Zhang, T. Xu, Z.X. Xie, L.S. Zheng, Controlling morphologies and tuning the related properties of nano/microstructured ZnO crystallites, Journal of Physical Chemistry: C 113 (2009) 584–589.
[35] Z. Deng, M. Chen, G. Gu, L. Wu, A Facile method to fabricate ZnO hollow spheres and their photocatalytic property, Journal of Physical Chemistry: B 112 (2008) 16–22.
[36] H. Wang, C. Xie, W. Zhang, S. Cai, Z. Yang, Y. Gui, Comparison of dye degradation efficiency using ZnO powders with various size scales, Journal of Hazardous Materials 141 (2007) 645–652.
[37] J. Ya Qi, L. Fang Fang, S. Ran, X. Zhao Xiong, Z. Lan Sun, A simple solvothermal route towards the morphological control of ZnO and tuning of its optical and photocatalytic properties, Science China Chemistry 53 (2010) 1711–1717.
[38] W.D. Zhou, X. Wu, Y.C. Zhang, M. Zhang, Solvothermal synthesis of hexagonal ZnO nanorods and their photoluminescence properties, Materials Letters 61 (2007) 2054–2057.
[39] W.B. Chang, K.A. Li, Concise Handbook of Analytical Chemistry, Beijing University Publishing Company, Beijing, 1981 (in Chinese).
[40] T. Kawano, H. Imai, Fabrication of ZnO nanoparticles with various aspect ratios through acidic and basic routes, Crystal Growth and Design 6 (2006) 1054–1056.
[41] A. Pan, R. Yu, S. Xie, ZnO flowers made up of thin nanosheets and their optical properties, Journal of Crystal Growth 282 (2005) 165–172.
[42] J. Du, Z. Liu, Y. Huang, Y. Gao, B. Han, W. Li, G. Yang, Control of ZnO morphologies via surfactants assisted route in the subcritical water, Journal of Crystal Growth 280 (2005) 126–134.
[43] W.J. Li, E.W. Shi, W.Z. Zhong, Z.W. Yin, Growth mechanism and growth habit of oxide crystals, Journal of Crystal Growth 203 (1999) 186–196.
[44] B. Liu, H.C. Zeng, Hydrothermal synthesis of ZnO nanorods in the diameter regime of 50 nm, Journal of the American Chemical Society 125 (2003) 4430–4431.
[45] C. Berberidou, I. Poulios, N.P. Xekoukoulotakis, D. Mantzavinos, Sonolytic, photocatalytic and sonophotocatalytic degradation of malachite green in aqueous solutions, Applied Catalysis B: Environmental 74 (2007) 63–72.
[46] A.J. Hoffman, E.R. Carraway, M.R. Hoffmann, Photocatalytic production of H_2O_2 and organic peroxides on quantum-sized semiconductor colloids, Environmental Science & Technology 28 (1994) 776–785.
[47] I. Hua, M.R. Hoffmann, Optimization of ultrasonic irradiation as an advanced oxidation technology, Environmental Science & Technology 31 (1997) 2237–2243.
[48] T. Wu, G. Liu, J. Zhao, H. Hidaka, N. Serpone, Evidence for H_2O_2 generation during the TiO_2-assisted photodegradation of dyes in aqueous dispersions under visible light illumination, Journal of Physical Chemistry B 103 (1999) 4862–4867.
[49] P.R. Gogate, A.B. Pandit, A review of imperative technologies for wastewater treatment II: hybrid methods, Advances in Environmental Research 8 (2004) 553–579.
[50] J. Zhang, L. Sun, J. Yin, H. Su, C. Liao, C. Yan, Control of ZnO morphology via a simple solution route, Chemistry of Materials 14 (2002) 4172–4177.
[51] Z. Wang, Zinc oxide nanostructures: growth, properties and applications, Journal of Physics: Condensed Matter 16 (2004) R829–R858.
[52] Q. Zhao, H. Zhang, Y. Zhu, S. Feng, X. Sun, J. Xu, D. Yu, Morphological effects on the field emission of ZnO nanorod arrays, Applied Physics Letters 86 (2005) 20311–203117.
[53] S.K. Kavitha, P.N. Palanisamy, Photocatalytic and sonophotocatalytic degradation of Reactive Red 120 using dye sensitized TiO_2 under visible light, Engineering and Technology 73 (2011) 1–6.
[54] H.K. Singh, M. Saquib, M. Haque, M. Muneera, D. Bahnemann, Titanium dioxide mediated photocatalysed degradation of phenoxyacetic acid and 2,4,5-trichlorophenoxyacetic acid, in aqueous suspensions, Journal of Molecular Catalysis A: Chemical 264 (2007) 66–72.
[55] M.M. Haque, M. Muneer, D.W. Bahnemann, Semiconductor-mediated photocatalyzed degradation of a herbicide derivative, chlorotoluron, in aqueous suspensions, Environmental Science and Technology 40 (2006) 4765–4770.
[56] B. Neppolian, H.C. Choi, S. Sakthivel, B. Arabindoo, V. Murugesan, Solar light induced and TiO_2 assisted degradation of textile dye reactive blue 4, Chemosphere 46 (2002) 1173–1181.
[57] A. Bianco-Prevot, C. Baiocchi, M.C. Brussino, E. Pramauro, P. Savarino, V. Augugliaro, G. Marci, L. Palmisano, Photocatalytic degradation of Acid Blue 80 in aqueous solutions containing TiO_2 suspensions, Environmental Science and Technology 35 (2001) 971–976.
[58] C. Galindo, P. Jacques, A. Kalt, Photodegradation of the aminoazobenzene acid orange 52 by three advanced oxidation processes: UV/H_2O_2, UV/TiO_2 and VIS/TiO_2: comparative mechanistic and kinetic investigations, Journal of Photochemistry and Photobiology A: Chemistry 130 (2000) 35–47.
[59] H. Zhan, H. Tian, Photocatalytic degradation of acid azo dyes in aqueous TiO_2 suspension I. The effect of substituents, Dyes and Pigments 37 (1998) 231–239.
[60] J. Bandara, J.A. Mielczarski, J. Kiwi, Photosensitized degradation of azo dyes on Fe, Ti, and Al oxides: mechanism of charge transfer during the degradation, Langmuir 15 (1999) 7680–7687.
[61] K. Tanaka, K. Padermpole, T. Hisanaga, Photocatalytic degradation of commercial azo dyes, Water Research 34 (2000) 327–333.
[62] I.K. Konstantinou, T.A. Albanis, TiO_2-assisted photocatalytic degradation of azo dyes in aqueous solution: kinetic and mechanistic investigations: a review, Applied Catalysis B: Environmental 49 (2004) 1–14.
[63] M.R. Hoffmann, S.T. Martin, W. Choi, D.W. Bahenemann, Environmental applications of semiconductor photo-catalysis, Chemical Review 95 (1995) 69–96.
[64] C. Nasr, K. Vinodgopal, S. Hotchandani, A. Chattopadhyaya, P.V. Kamat, Environmental photochemistry on semiconductor surfaces, Journal of Physical Chemistry 100 (1996) 8436–8442.
[65] K. Vinodgopal, D.E. Wynkoop, P.V. Kamat, Environmental photochemistry on semiconductor surfaces: Photosensitized degradation of a textile azo dye, Acid Orange 7, on TiO_2 particles using visible light, Environmental Science and Technology 30 (1996) 1660–1666.
[66] C. Bauer, P. Jacques, A. Kalt, Investigation of the interaction between a sulfonated azo dye (AO7) and a TiO_2 surface, Chemical Physics Letters 307 (1999) 397–404.